



HAL
open science

Assimilation of AIRS Radiances Affected by Mid- to Low-Level Clouds

Thomas Pangaud, Nadia Fourrié, Vincent Guidard, Mohamed Dahoui,
Florence Rabier

► **To cite this version:**

Thomas Pangaud, Nadia Fourrié, Vincent Guidard, Mohamed Dahoui, Florence Rabier. Assimilation of AIRS Radiances Affected by Mid- to Low-Level Clouds. *Monthly Weather Review*, 2009, 137 (12), pp.4276-4292. meteo-00564268

HAL Id: meteo-00564268

<https://meteofrance.hal.science/meteo-00564268>

Submitted on 4 Mar 2022

HAL is a multi-disciplinary open access archive for the deposit and dissemination of scientific research documents, whether they are published or not. The documents may come from teaching and research institutions in France or abroad, or from public or private research centers.

L'archive ouverte pluridisciplinaire **HAL**, est destinée au dépôt et à la diffusion de documents scientifiques de niveau recherche, publiés ou non, émanant des établissements d'enseignement et de recherche français ou étrangers, des laboratoires publics ou privés.



Distributed under a Creative Commons Attribution 4.0 International License

Assimilation of AIRS Radiances Affected by Mid- to Low-Level Clouds

THOMAS PANGAUD, NADIA FOURRIE, AND VINCENT GUIDARD

CNRM-GAME, Météo-France, and CNRS, Toulouse, France

MOHAMED DAHOUI

European Centre for Medium-Range Weather Forecasts, Reading, United Kingdom

FLORENCE RABIER

CNRM-GAME, Météo-France, and CNRS, Toulouse, France

(Manuscript received 30 March 2009, in final form 10 June 2009)

ABSTRACT

An approach to make use of Atmospheric Infrared Sounder (AIRS) cloud-affected infrared radiances has been developed at Météo-France in the context of the global numerical weather prediction model. The method is based on (i) the detection and the characterization of clouds by the CO₂-slicing algorithm and (ii) the identification of clear–cloudy channels using the ECMWF cloud-detection scheme. Once a hypothetical cloud-affected pixel is detected by the CO₂-slicing scheme, the cloud-top pressure and the effective cloud fraction are provided to the radiative transfer model simultaneously with other atmospheric variables to simulate cloud-affected radiances. Furthermore, the ECMWF scheme flags each channel of the pixel as clear or cloudy. In the current configuration of the assimilation scheme, channels affected by clouds whose cloud-top pressure ranges between 600 and 950 hPa are assimilated over sea in addition to clear channels. Results of assimilation experiments are presented. On average, 3.5% of additional pixels are assimilated over the globe but additional assimilated channels are much more numerous for mid- to high latitudes (10% of additional assimilated channels on average). Encouraging results are found in the quality of the analyses: background departures of AIRS observations are reduced, especially for surface channels, which are globally 4 times smaller, and the analysis better fits some conventional and satellite data. Global forecasts are slightly improved for the geopotential field. These improvements are significant up to the 72-h forecast range. Predictability improvements have been obtained for a case study: a low pressure system that affected the southeastern part of Italy in September 2006. The trajectory, intensity, and the whole development of the cyclogenesis are better predicted, whatever the forecast range, for this case study.

1. Introduction

The Atmospheric Infrared Sounder (AIRS) on board the *Aqua* satellite (Aumann et al. 2003) belongs to a new generation of advanced satellite sounding instruments that provide information about atmospheric temperature and humidity profiles with a spectral resolution far exceeding that of previous sounders such as the High Resolution Infrared Radiation Sounder (HIRS). The Infrared Atmospheric Sounder Interferometer (IASI) on board the *MetOp* satellite (Cayla 2001) with a better

spectral resolution than AIRS, also belongs to this new generation of advanced satellite sounding instruments. These highly informative observations are used to improve numerical weather prediction (NWP) analysis and forecast accuracy.

A large amount of measurements from advanced infrared sounders are affected by clouds [i.e., 90% according to Fourrié and Rabier (2004)] and cloud-contaminated observations are currently rejected by the data assimilation system due to deficiencies in the representation of cloud processes. Since clouds affect the infrared satellite observations, clouds have to be detected before data are assimilated. Indeed, unfiltered cloud-affected observations can have a negative impact on the quality of NWP analyses if they are assimilated as clear observations.

Corresponding author address: Thomas Pangaud, Météo-France, 42 avenue Gaspard, Coriolis, Toulouse CEDEX 31057, France.
E-mail: thomas.pangaud@cnrm.meteo.fr

Several cloud-detection schemes have been used: the most conservative method consists in rejecting all fields of view classified as cloudy (English et al. 1999) and then only to focus on completely clear locations. This technique leads to a yield in terms of exploited soundings of about 5% (Pavelin et al. 2008). Another technique developed at the European Centre for Medium-Range Weather Forecasts (ECMWF) by McNally and Watts (2003), hereinafter called the ECMWF scheme, is based on the detection of cloud-affected channels and consists in using only channels that are thought to be unaffected by clouds, inside clear or cloud-affected soundings. The yield in terms of exploited sounders is higher than by the previous method and the benefit in terms of additional assimilated channels is far from being negligible (McNally and Watts 2003). However, only a small proportion of the available soundings is being exploited, especially for tropospheric channels: roughly 15% for a stratospheric channel and 8% for an upper-tropospheric channel. A third alternative approach, the so-called cloud-clearing method, consists in simulating a clear observation by using multiple fields of view and assuming that only cloud fraction changes between these adjacent fields of view (Eyre and Watts 1987; Li et al. 2005), but the assumption of homogeneous cloud characteristics is not verified in the majority of cases (Pavelin et al. 2008) and the successful exploitation of cloud-cleared radiances by NWP is thus not obvious.

Nevertheless, the assimilation of only clear observations can lead to a poor description of some particular atmospheric situations such as regions with high humidity (e.g., low-latitude regions). Finally, it is well known that the sensitive regions, where cyclogenesis start to develop, are often cloudy (McNally 2002). The underexploitation of advanced sounders and the wish to better describe the atmosphere and to limit forecast error growth in sensitive regions motivate our research efforts to assimilate cloud-affected radiances. The observed radiance spectra that contain temperature and humidity information can also provide information on clouds. Two main methods are actually investigated in NWP centers to deal with cloud-affected infrared radiances: the first approach is based on the insertion of a physical cloud scheme into the observation operator. An approach based on a diagnostic cloud scheme has been tested by ECMWF, for instance, with an encouraging impact on temperature and humidity fields (Chevallier et al. 2004). This diagnostic cloud scheme estimates cloud parameters from the model variables: a cloud is assumed here to be a multilayer gray body. A radiative transfer model (RTM) is used as an observation operator, then it simulates cloud-affected radiances. The second approach is based on the use of the cloud-

top pressure (CTP) and the effective cloud fraction N_e calculated by a cloud-characterization algorithm. These parameters are then provided to the RTM to simulate cloud-affected radiances. Several techniques are commonly used to retrieve cloud parameters from radiance measurements, such as the minimum residual method (Eyre and Menzel 1989). Pavelin et al. (2008) have demonstrated that a one-dimensional variational data assimilation (1D-Var) processing of CTP and N_e before being used by the RTM results in a more accurate cloud parameter retrieval. This approach constitutes the operational configuration at the Met Office to assimilate AIRS cloud-affected radiances.

For the purpose of this study, cloud parameters are estimated with the second above-described approach. This method has been chosen because preliminary cloud-affected radiance assimilation experiments have shown that this method leads to promising impacts on analysis and forecast (Dahoui 2006). It also presents the vantage to provide a better computational efficiency. The cloud parameter retrieval scheme used in this study is the CO₂-slicing method based on radiative transfer principles (Chahine 1974; Menzel et al. 1983). The RTM used is a fast RTM, the 8.5 version of the Radiative Transfer for Television and Infrared Observation Satellite (TIROS) Operational Vertical Sounder (RTTOV), which is the operational version of RTTOV at Météo-France (Saunders et al. 2002). In this framework, once a hypothetical cloud-affected pixel is detected by the CO₂-slicing scheme and its parameters are retrieved, the cloud-affected radiances are simulated by RTTOV. Furthermore, channels of this pixel are flagged to be clear or cloudy by the ECMWF scheme. Finally, cloud-affected channels whose CTP is included between 600 and 950 hPa, and clear channels are assimilated over the sea in the French NWP global model, Action de Recherche Petite Echelle Grande Echelle (ARPEGE) through a four-dimensional variational data assimilation (4D-Var) scheme. Our assimilation period, which includes among others a strong mesoscale storm in the Mediterranean Sea, begins at 0000 UTC 1 September 2006 and ends at 1800 UTC 30 September 2006. At that time, the *MetOp* satellite was not launched yet and IASI data were thus not available. For this reason, the processing of IASI has not been mentioned in this paper and we have just focused on AIRS data processing.

The plan of this paper is as follows. Section 2 focuses on a brief description and evaluation of two cloud-detection schemes applied to AIRS: the ECMWF and the CO₂-slicing scheme. The method used to directly assimilate cloud-affected radiances in the 4D-Var assimilation scheme of ARPEGE is presented in section 3. Experiments assimilating clear and cloudy AIRS radiances have

been performed. Section 4 focuses on these experiments in terms of AIRS observation usage and characterization. Results in terms of impact on the quality of the analysis and on the skill of the forecasts are discussed in section 5. Finally the impact on the forecast is further evaluated in a case study of a strong mesoscale storm in section 6. Concluding remarks follow in section 7.

2. Evaluation of AIRS cloud-detection schemes

a. AIRS cloud-detection schemes

1) ECMWF SCHEME

The ECMWF scheme (McNally and Watts 2003) aims at detecting clear channels within a measured spectrum rather than the detection of totally clear pixels. If the background spectrum (defined as the spectrum computed from the best available background estimate of the atmospheric state) is close enough to the true state of the atmosphere, the cloud signature is identified by the first-guess departure of the observed spectrum from clear-sky background values. The term “background” represents here a short-range NWP forecast (6 h) from the previous analysis. In this study, a set of 319 channels, chosen among the 324 available ones in real time to NWP users, is used. Channels are first reordered into a vertically ranked space according to the lower tail of their respective weighting function. The ranking consists in assigning to each channel, a pressure level (in RTTOV coordinates) at which the radiation effect of a one-layer blackbody is less than 1%. A low-pass filter is then applied to the ranked departures to reduce the instrument noise and the cloud emissivity effect. Finally, a search for the channel at which a monotonically growing departure can first be detected, determines the first significant cloud contamination. Once this channel is found, all other less sensitive channels are flagged cloud free and the more sensitive ones are flagged cloudy. A pixel is declared clear if all of the 319 channels are flagged cloud free.

2) CO₂-SLICING SCHEME

The CO₂-slicing method (Chahine 1974; Menzel et al. 1983), based on radiative transfer principles, is widely used to retrieve CTP and N_e . Here N_e conceptually represents the product of the geometrical cloud fraction and the gray body emissivity of the cloud. This method uses a simplistic cloud model: the cloud is considered as a single layer of opaque or semitransparent thin cloud with a homogeneous emissivity. The algorithm uses observed radiances of a set of 124 AIRS channels selected in the CO₂ absorption band (between 649.612 and 843.913 cm⁻¹), which is very sensitive to clouds. For

each AIRS pixel, and each channel in the set, the following function is calculated:

$$F_{k,p} = \frac{(R_{\text{clear}}^k - R_{\text{meas}}^k)}{(R_{\text{clear}}^{k_{\text{ref}}} - R_{\text{meas}}^{k_{\text{ref}}})} - \frac{(R_{\text{clear}}^k - R_{\text{cld}}^{k,p})}{(R_{\text{clear}}^{k_{\text{ref}}} - R_{\text{cld}}^{k_{\text{ref}},p})}, \quad (1)$$

where p is the pressure level number, k is the channel in the CO₂ band, k_{ref} represents the reference window channel (979.1279 cm⁻¹), R_{meas}^k is the measured radiance for channel k , R_{clear}^k is the simulated clear radiance for channel k , and $R_{\text{cld}}^{k,p}$ represents the simulated blackbody radiance for channel k at the cloud level p . The cloud-top pressure level assigned to each channel k is the pressure level $p_{c,k}$, which minimizes the function $F_{k,p}$. Before ascertaining the CTP of a hypothetical cloud, a filter that distinguishes channels with δTBs (difference between observed brightness temperature and simulated brightness temperature) lower than the radiometric noise is applied to the algorithm. If all channels are filtered out, the pixel is flagged clear. If the pixel is cloud contaminated, the CTP is then calculated by the following expression:

$$\text{CTP} = \frac{\sum p_{c,k} w_k^2}{\sum w_k^2}, \quad (2)$$

where $w_k = \delta F_{k,p} / \delta \ln p$ is the derivative of the cloud pressure function.

The effective cloud fraction is obtained for the reference window channel by the following expression:

$$N_e = \frac{(R_{\text{clear}}^{k_{\text{ref}}} - R_{\text{meas}}^{k_{\text{ref}}})}{(R_{\text{clear}}^{k_{\text{ref}}} - R_{\text{cld}}^{k_{\text{ref}},p_c})}. \quad (3)$$

If the algorithm produces a retrieved N_e smaller than 0.1, the pixel is flagged clear. Both above-calculated parameters are used by RTTOV to simulate cloud-affected radiances.

b. Results and discussion

The evaluation of both cloud-detection schemes is fundamental as unfiltered cloud-affected observations can have a detrimental impact on the quality of the analysis if they are assimilated as clear. For this study, a cloud-characterization product based on the Moderate Resolution Imaging Spectroradiometer (MODIS) data has been used as a reference. The MODIS imager is a key instrument on board the Earth Observation System satellites. We have used data product collected from the *Aqua* platform from the Interactions Clouds Aerosols Radiations Etc. (ICARE) center (more information available online at http://www.icare.univ-lille1.fr/archive/archive.php?dir=MODIS/MYD06_L2/), which

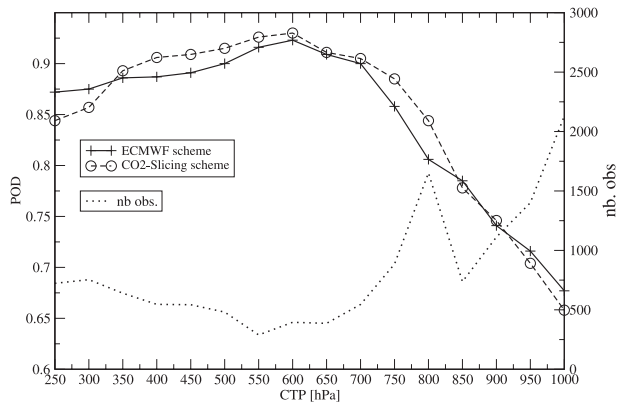


FIG. 1. Efficiency of the cloud detection according to the retrieved cloud-top pressure from MODIS. Evaluation period lasted from 1 to 10 Sep 2006. The CO₂ slicing is represented by a dashed line with circles and the ECMWF scheme is represented by a solid line with crosses. The number of observations is represented by the dotted line.

are produced at an horizontal resolution of 5 km at nadir and cover a 5-min time interval. Because of downloading resource limitations, the comparison is limited to the Atlantic region. The validation is performed within a 10-day period: from 1 to 10 September 2006. A total of 15 706 AIRS pixels have been processed. As the evaluation of both cloud-detection schemes has already been performed (Dahoui et al. 2005) and results are briefly discussed in this paper.

Performances for both schemes are similar in terms of detection of cloudy and clear pixels. These results confirm previous studies (Dahoui et al. 2005). Figure 1 highlights the accuracy of the cloud detection for the CO₂-slicing and the ECMWF schemes for several ranges of CTP inferred from MODIS. The detection of medium clouds (between 400 and 800 hPa) delivers the best results. In contrast, the detection of low-level and high clouds (CTP > 800 hPa and CTP < 400 hPa, respectively) is not as efficient as for medium clouds for both schemes. For low-level clouds, this must be due to the similarity of the measured signal from clear-sky and low-cloud scenes in some particular situations which make the detection of these low clouds more difficult. Concerning high clouds, the problem is mostly due to the insensitivity of the sounding-based method to thin clouds (identical thresholds are applied for the detection of each type of clouds). Furthermore, clouds whose CTP varies between 250 and 300 hPa and those whose CTP varies between 900 and 1000 hPa are slightly better detected by the ECMWF scheme. Clouds whose CTP varies between 300 and 850 hPa are slightly better detected by the CO₂-slicing scheme.

The retrieved CTP from CO₂-slicing exhibits a correlation of about 0.79 with the CTP inferred from MODIS.

Correlation between the N_e retrieved from the CO₂-slicing scheme and the ones inferred from MODIS is quite low for each range of N_e (about 0.51). This low correlation may first be explained by the presence of clouds distributed in the vertical (which are assumed to be single-layer clouds by the RTTOV) whose radiative effect is comparable to a cloud with a higher cloud fraction located at a single level. Moreover, the relative bad detection of low clouds that exhibit a low contrast with the surface in some particular situations may also account for this low correlation. These CTP and N_e correlations are of the same order of magnitude as those found by Pavelin et al. (2008) with the minimum residual method: between 0.67 and 0.81 for the CTP and between 0.46 and 0.78 for the N_e .

3. Framework of the study

a. Methods to determine background cloud parameters

The observation operator used here for the assimilation of cloud-contaminated radiances is the 8.5 version of RTTOV, complemented by horizontal and vertical interpolations. It simulates infrared and microwave radiances observed by satellite sounders (Saunders et al. 2002). For each channel, the optical depth is obtained from linear regressions based on RTTOV input variables: temperature and humidity profiles and surface data. Although RTTOV has initially been designed to be used in clear-sky conditions, it is able to simulate cloud-contaminated radiances. The radiative transfer in cloudy conditions can be performed by two different techniques:

- The cloud is assumed to be a single-layer blackbody of negligible depth that CTP has been provided to the RTM. The cloud-affected radiance is calculated using the following expression:

$$R_{\nu}^{\text{clld}}(\theta) = B_{\nu}[T(z_{\text{clld}})]\tau_{\nu}(z_{\text{clld}}, \theta) + \int_{z_{\text{clld}}}^{\infty} B_{\nu}[T(z)][d\tau_{\nu}(z, \theta) dz]/dz, \quad (4)$$

where $R_{\nu}^{\text{clld}}(\theta)$ is the cloudy monochromatic radiance of frequency ν going away from the top of the cloud toward space with an incidence angle θ , $\tau_{\nu}(z_{\text{clld}}, \theta)$ represents the transmittance between the cloud top and space, $T(z_{\text{clld}})$ represents the cloud-top temperature, $T(z)$ is the temperature of an atmospheric layer at altitude z , and B_{ν} represents the Planck function. Equation (4) defines the overcast radiance. In reality, most of the pixels are partially cloud contaminated.

These kinds of pixels are defined by a linear blending of overcast and clear radiances using the following equation:

$$R_v(\theta) = (1 - N)R_v^{\text{clr}}(\theta) + NR_v^{\text{clld}}(\theta), \quad (5)$$

where $R_v^{\text{clr}}(\theta)$ represents the clear-sky component of the radiance and N represents the cloud cover.

- A more realistic multilayer parameterization of clouds is in the RTTOVCLD module: clouds are defined by several vertical levels and for different cloud water phases (liquid or ice) from vertical profiles provided to the RTM (temperature profiles, humidity, cloud cover, liquid cloud water, and cloud ice) by a physical cloud scheme. Clouds are assumed to be multilayer gray bodies.

We made the choice to use the first method although the use of a physical cloud scheme (second method) is potentially valuable (Chevallier et al. 2004). Unfortunately, the physics of the model in its current state is far from the required accuracy. According to Dahoui (2006), the first method provides a better computational efficiency and leads to promising impacts on analysis and forecast. The cloud emissivity is assumed to be equal to 1, which is acceptable for thick opaque clouds but not valid for thin clouds like cirrus. The latter are high clouds whose impact is not taken into account in our assimilation scheme (as only radiances affected by mid- to low-level clouds are treated here). Thus, this assumption has no impact in the simulation of cloud-affected radiances in this study context.

b. Experiment setup

The NWP model used in this work is ARPEGE (Courtier et al. 1991), which is the Météo-France operational global model. It uses a stretched grid with a horizontal resolution of 23 km over France and 133 km over the antipodes. The assimilation scheme is a 4D-Var assimilation (Courtier et al. 1994; Rabier et al. 2000). It uses the following data sources: land surface stations, sea surface station (drifting buoys, ship reports, etc.), aircraft data, in situ sounding data (radiosonde and pilot balloon reports, etc.), wind profiler radar data, Global Positioning System (GPS) ground-based data, geostationary satellite winds (atmospheric motion vectors), and polar-orbiting satellite radiances and winds. Radiances from polar-orbiting satellites provide ARPEGE with roughly 50% of the total volume of assimilated data. AIRS data represented roughly 65% of the volume of polar-orbiting satellite data and more than 30% of the total volume of assimilated data. All these data sources are subject

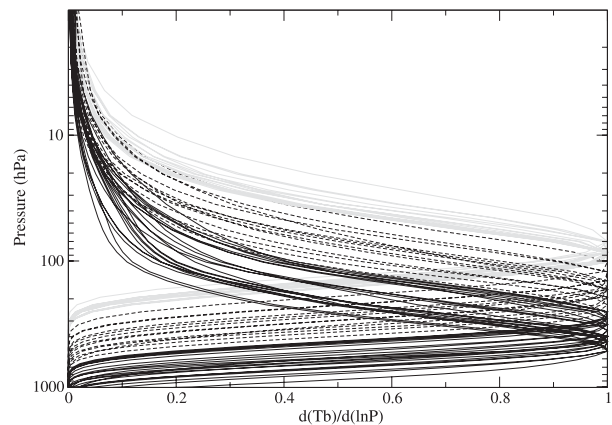


FIG. 2. Weighting functions of the 54 assimilated AIRS channels. Solid black lines represent tropospheric peaking channels, dashed lines represent tropopause peaking channels, and solid gray lines represent stratospheric peaking channels.

to various quality control checks and suspect ones are rejected. The quality control applied to AIRS is based on differences between observations and background values, with a rejection of the observation if the difference is larger than a given threshold. Moreover, a geographical thinning of 250 km is applied to all radiance data. Satellite data are bias corrected with an adaptive variational method (viz., VarBC), using geometric and flow-dependent predictors to remove systematic errors in satellite radiance data (Dee 2004; Auligné et al. 2007). In this study, three types of predictors were used: a global offset applied to each channel, a scan angle correction based on the nadir-viewing angle (to the power of 1, 2, and 3) and an air mass correction (predictors are the four atmospheric thicknesses 1000–300, 200–50, 10–1, and 50–5 hPa). We have used the operational subset of 54 channels located in the temperature longwave band chosen among the 324 channels available on the Global Transmission System. This subset contains 19 stratospheric channels with weighting functions peaking from 56 to 85 hPa, 12 channels with weighting functions peaking from 102 to 222 hPa sampling the tropopause, and 23 upper-tropospheric channels with weighting-functions peaking from 253 to 478 hPa (Fig. 2). These channels are only assimilated over seas. The assimilation period of this study covers a full month, from 1 to 30 September 2006. In this approach, once a cloud-affected pixel is detected by the CO₂-slicing scheme, cloud parameters (CTP and N_e) are retrieved from infrared radiance measurements out of the observation operator and are then directly used as inputs of RTTOV, which will then simulate the cloud-affected spectrum. Thus, N_e and CTP are determined at the beginning of the assimilation cycle with no adjustments during the minimization.

Furthermore, the ECMWF scheme identifies each channel of the pixel as clear or cloudy. Finally, channels affected by clouds whose CTP ranges between 600 and 950 hPa are assimilated together with clear ones and all other cloud-contaminated channels are rejected from the assimilation scheme. Two assimilation experiments have been run to test the impact of the direct assimilation of cloud-contaminated radiances: the first one is a reference experiment that only assimilates clear AIRS radiances with the others above-described data. This reference experiment is called REF in the following study. The second one assimilates cloud-affected radiances on top of clear radiances and other above-described data sources. In the following study this experiment is called EXP. The adaptive variational bias correction from REF is applied to both clear- and cloud-affected radiances in EXP. An experiment similar to EXP (figures not shown) has been run with its own adaptive bias correction but differences with EXP remain small (e.g., no drift in number of active assimilated observations). To disentangle effects of assimilating cloud-affected radiances from those of bias correction variation, only EXP is discussed in this paper.

c. Application for mid- to low-level clouds

As previously seen, cloud-affected radiances are assimilated here for clouds whose CTP is included between 600 and 950 hPa. On one hand, the rejection of clouds situated higher than 600 hPa is motivated by the assimilation of tropospheric channels (up to 478 hPa) into our assimilation scheme and only clouds situated lower than peaks of the weighting function are selected. Indeed, the assimilation of clouds situated higher than the weighting function peak of a given channel can lead to large biases and root-mean-square (RMS) errors for both background and analysis as shown by Pavelin et al. (2008). On the other hand, it has been shown in section 2b that the detection of low-level clouds ($800 < \text{CTP} < 950$) was not as efficient as the detection of higher clouds and their assimilation could thus appear delicate. A sensitivity study has been performed to check whether or not the AIRS spectrum was affected by the nondetection of these low clouds. It consists in comparing EXP (which simulates cloud-contaminated radiances) and REF (which only simulates clear radiances) averaged innovations (observations minus simulated radiances using the background state of the atmosphere) with respect to the channel number at a given CTP range (800–950, 600–800, 400–600, and 200–400 hPa) for all the observations (Fig. 3). The AIRS spectrum is almost not affected by the simulation inside RTTOV of clouds whose CTP is included between 800 and 950 hPa (Fig. 3a). Difficulties of cloud-detection schemes to detect some low clouds have thus a negligible impact on the background simu-

lation, contrary to other level clouds where the simulated AIRS spectrum is more affected by the simulation of clouds inside RTTOV (Figs. 3b–d). The assimilation of such low-level clouds is also motivated by the large number of retrieved CTP between 900 and 950 hPa (Fig. 4). However, very low clouds ($\text{CTP} > 950$ hPa) were rejected because the huge number of these cloud types (Fig. 4) does not seem physically plausible. The CO_2 slicing is obviously not able to accurately treat these very low clouds, most probably because of their weak impact on the signal measured by the sounder.

Our choice to assimilate cloud-affected channels whose CTP is included between 600 and 950 hPa appears thus to be a good compromise between, on one hand, the rejection of doubtful observations and those potentially spoiling the analysis, and, on the other hand, the assimilation of a nonnegligible volume of additional cloud-affected observations.

4. Impact on AIRS observations

a. Number and localization of additional assimilated observations

Figure 5 shows the number of active observations for each assimilated channel for the first assimilation window (0000 UTC 1 September 2006). This assimilation window is particularly interesting because the background used is the same for EXP and REF. The number of active observations is roughly the same for EXP and REF until channel 138, which is one of the first channels whose weighting function is pointing into the tropopause. Previous channels (from 15 to 117) are stratospheric channels, thus seldom cloud contaminated, and exhibit the same behavior for both experiments. Channels 138 to 251 are upper-tropospheric channels and are thus potentially contaminated by clouds. This hypothetical contamination leads to a rejection of these contaminated channels in REF whereas some of these contaminated channels are assimilated in EXP. The lower the channel points in the atmosphere, the larger the probability of a cloud contamination and the larger is the difference between the assimilated observation numbers for the two experiments. Furthermore, the number of active clear observations is lower for EXP than for REF for each tropospheric channel. This may be due to the geographical thinning of the assimilated pixels. This thinning is based on the maximum number of nonrejected channels (monitored and assimilated channels) per profile. REF keeps the profile with the maximum number of clear channels as cloud-contaminated channels are rejected from the assimilation. It is the opposite for EXP that has a maximum number of nonrejected channels in the profile in the

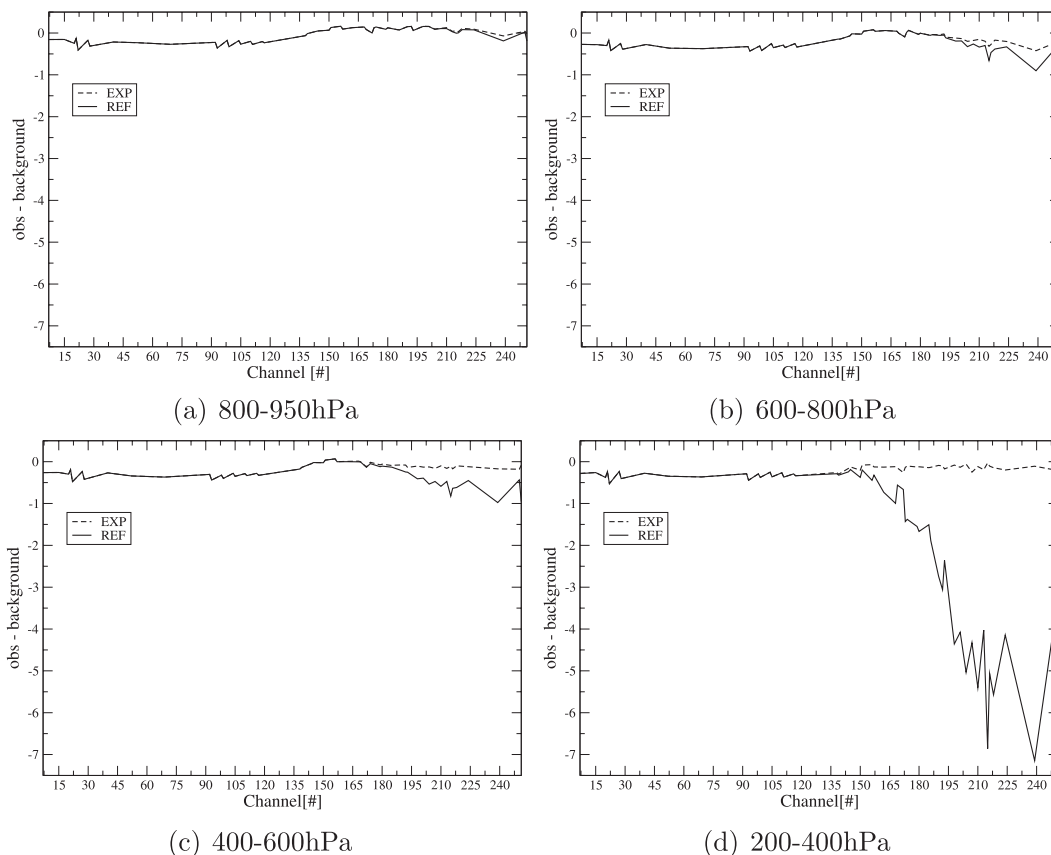


FIG. 3. Averaged innovations (observations—background) after bias correction of all observations for the 54 assimilated channels 2006 according to cloud-top pressure for 1 Sep. Solid line is for REF and dashed line is for EXP.

presence of a cloud whose CTP is between 600 and 950 hPa (in that case, all channels are nonrejected, except for the gross error).

Figures 6a,b, respectively, exhibit the number of assimilated pixels and assimilated channels (many channels are potentially assimilated in a given pixel) for both experiments with respect to their latitudinal position and for the whole study period. Most of the active pixels and channels are situated in the Southern Hemisphere, which is consistent with the assimilation of overseas observations (the oceanic surface is larger in the Southern Hemisphere than in the Northern Hemisphere). EXP assimilates between 1% and 4% more pixels than REF (Fig. 6a) with a slightly larger rate at mid- to high latitudes. The 250-km geographical thinning restricts these rates that would be higher if the geographical density of assimilated radiances were higher. The difference of assimilated channels between EXP and REF in mid- to high latitudes (Fig. 6b) is much larger than the difference of assimilated pixels (Fig. 6a): on average, 10% of additional channels against 3.5% of additional pixels. These differences are not visible for low latitudes (1.5% of

additional pixels and channels on average). Thus, even if the assimilation of cloud-affected radiances yields additional active pixels to ARPEGE with quite a uniform repartition on the globe, the additional information is

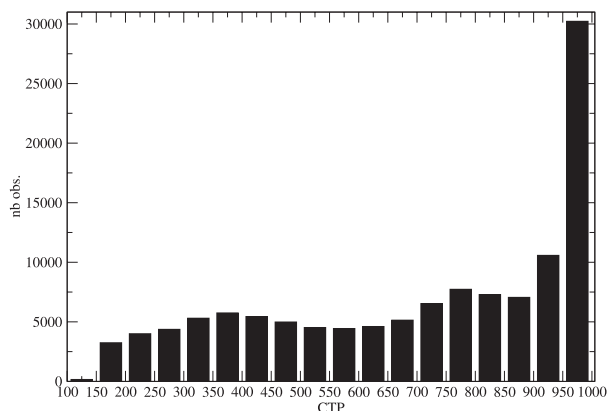


FIG. 4. Distribution of cloud-top pressure retrieved from CO₂ slicing on AIRS cloud-affected pixels ($N_e > 0.1$) used in the validation period (1–10 Sep 2006).

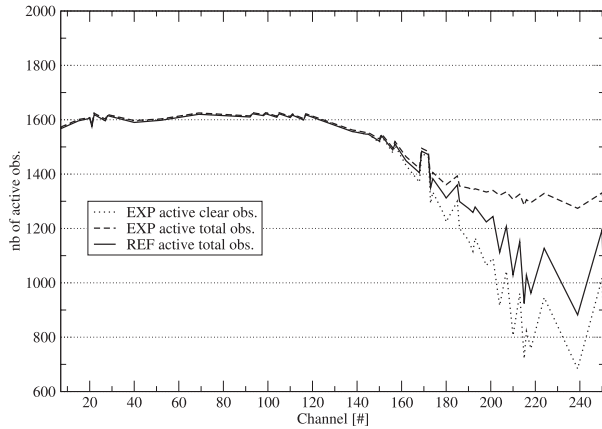


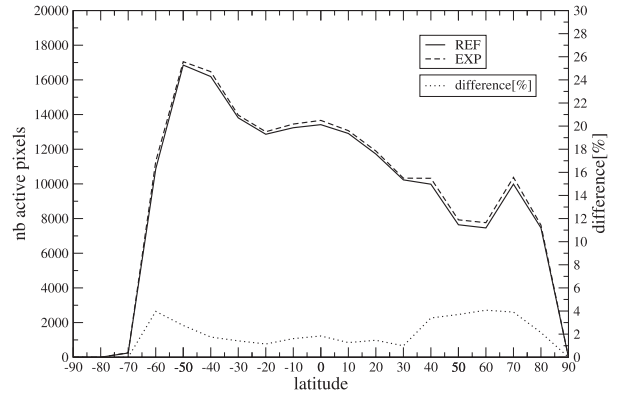
FIG. 5. Number of active channels at 0000 UTC 1 Sep 2006 with respect to channel number. The total number of active channels of REF is represented by the solid line, the total number of active channels of EXP is represented by the dashed line, and the number of active clear channels of EXP is represented by the dotted line.

much larger for mid- to high latitudes than for low latitudes. This could be due to the nonassimilation of high-level clouds (CTP < 600 hPa) that are most frequent in the tropics [see the International Satellite Cloud Climatology Project (ISCCP) Web site online at <http://isccp.giss.nasa.gov>].

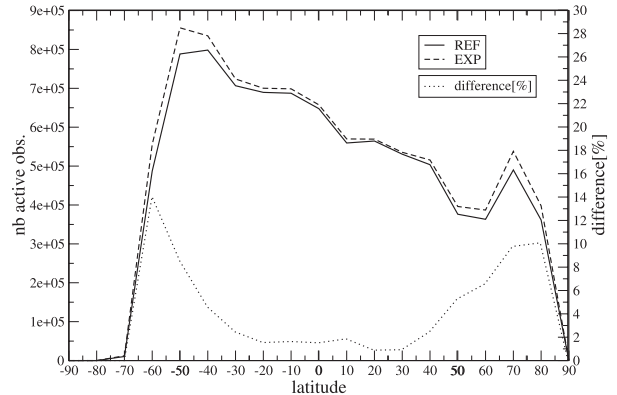
The daily evolution of the number of assimilated observations has also been studied at 1200 UTC (not shown) for assimilated channels peaking at the tropopause, upper troposphere, and midtroposphere in order to check whether the quality control was stable all along the assimilation period. For these channels, the number of active observations is constant for both experiments all along the study period, which proves that the quality control (and the cloud detection) is reliable.

b. Residual bias of observations

Figure 7a compares innovations of REF and EXP for each channel and for all observations (used and rejected observations) for the first assimilation window. Only the impact of the brightness temperature simulation by CO₂ slicing is thus seen in this figure. Innovation amplitudes fluctuate from -8 to 3 K for REF, with an absolute amplitude maximum for longwave surface peaking channels (from 759.6 to 1030.5 cm⁻¹ and from 1061.8 to 1135.6 cm⁻¹) and from 1.5 to 4 K for EXP (with an isolated peak at -5.5 K for channels 72 and 73). Innovations obtained by EXP are thus globally 4 times smaller than the ones obtained by REF for surface channels. It globally represents a cooling of the background estimation of about 6 K. Another significant cooling (from 6 to 3 K) is observed for lower-tropospheric peaking channels sensitive to water vapor (from 1218.5 to 1392.2 cm⁻¹). A smaller



(a) Active pixels.



(b) Active channels.

FIG. 6. Geographical distribution of (a) active pixels and (b) active channels with respect to latitude over the entire assimilation period (1–30 Sep 2006). The solid line represents EXP and the dashed line represents REF. The difference (%) between both experiments is the dotted line.

cooling (1–2 K) is observed for upper-tropospheric peaking channels sensitive to water vapor (from 1397.1 to 1605.1 cm⁻¹). Each shortwave channel (except shortwave stratospheric channels) presents also a significant cooling of about 4 K (from 2181.9 to 2298.7 cm⁻¹ and from 2380.4 to 2664.1 cm⁻¹). These differences show that to take into account cloud parameters into the radiative transfer calculations leads to model equivalents more consistent with observations. Figure 7b is a zoom on the active channel part of the previous figure. Innovations for EXP and REF are similar from 651.1 to 701.1 cm⁻¹ (stratospheric channels). Innovation amplitude differences are larger from 702.5 to 721.5 cm⁻¹, which are tropospheric peaking channels and are potentially more cloud contaminated. We have verified for the last day of our assimilation period (30 September 2006) at 0000 UTC that the variational bias correction was efficient throughout the assimilation period: innovation amplitudes are of the same order than those observed in the first assimilation window for both experiments.

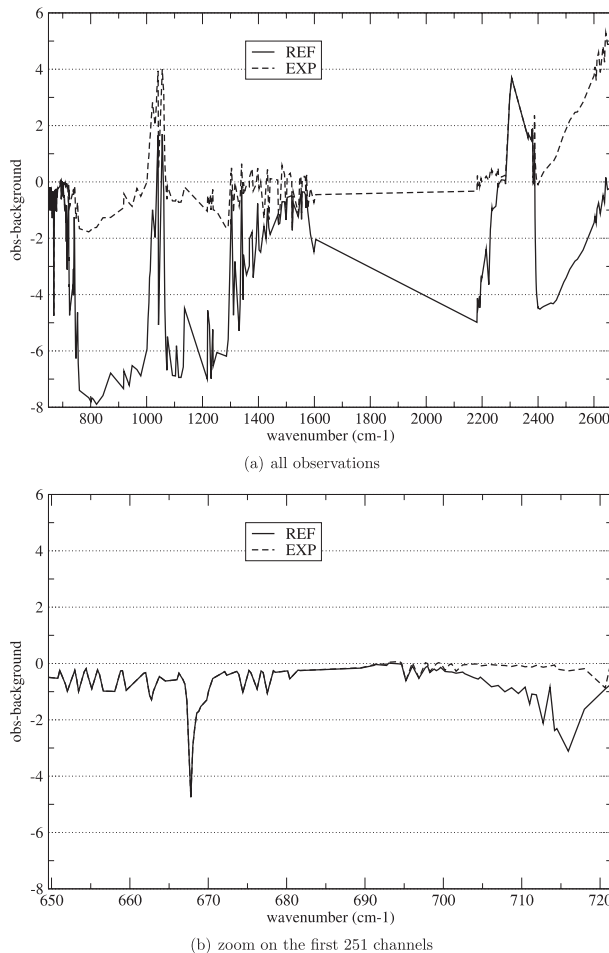


FIG. 7. Averaged innovations (observations–background) of all observations for the 324 available AIRS channels at 0000 UTC 1 Sep 2006. REF is represented by the solid line and EXP by the dashed line.

5. Impact on analysis and forecasts

a. Impact on analysis

EXP and REF statistics (differences in terms of biases and RMS) from various types of assimilated observations (conventional and satellite data) have been studied over the whole assimilation period. Both background and analysis statistics are in the majority of cases equivalent for both EXP and REF (not shown), but slight improvements have been noticed. With regards to conventional data, a slight reduction of, respectively, the bias and the RMS is observed for winds from profilers in the stratosphere over the Southern Hemisphere and in the upper-troposphere over the Northern Hemisphere. Regarding satellite data, a better fit to microwave sounders sensitive to atmospheric humidity has been noticed: analysis and background bias reduction for the Special Sensor Microwave Imager (SSM/I) in the

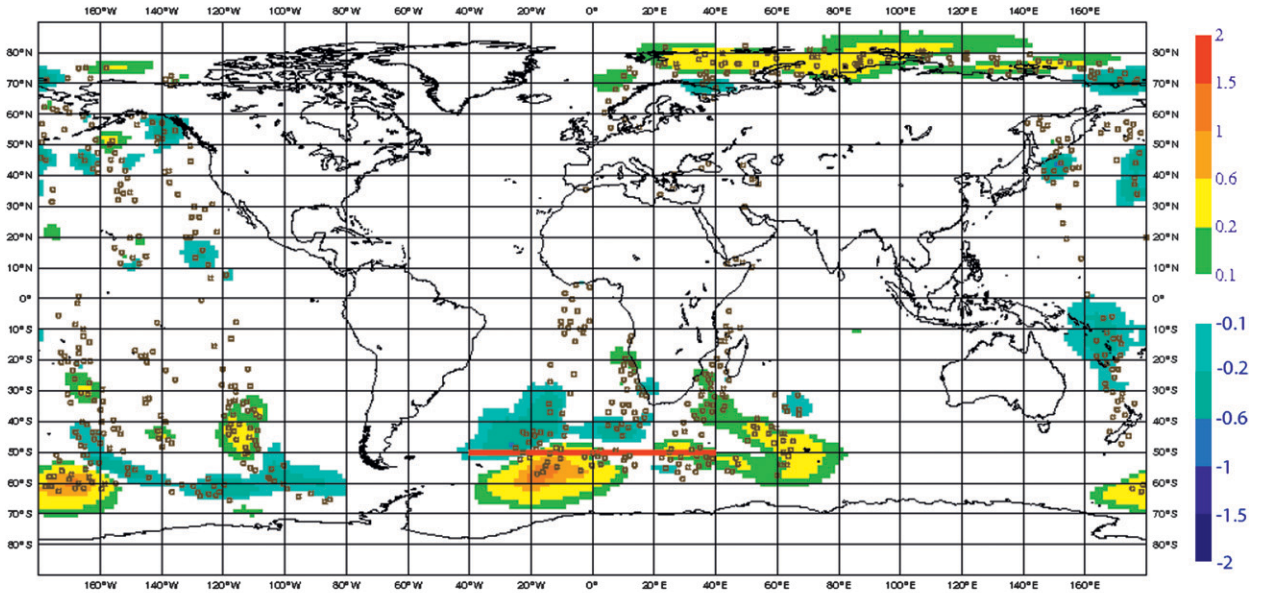
tropics and over the Southern Hemisphere in the wider atmosphere and a background bias reduction of mid-tropospheric channels of the Advanced Microwave Sounding Unit-B (AMSU-B) in the tropics.

Figure 8a highlights differences between EXP and REF analyses for the temperature at 500 hPa for the first analysis. Differences in model fields are, as expected, located in places where cloud-affected observations are assimilated in EXP showing that these differences are mainly due to the assimilation of cloud-affected observations. These differences are globally located in the Northern Hemisphere between 40° and 90°N and in the Southern Hemisphere between 30° and 70°S. By contrast, the intertropical zone is almost not affected by the assimilation of cloud-affected observations. Furthermore, our assimilation period spreads out the austral winter, where oceans below 70°S are fully covered by sea ice, which is not the case for oceans above 70°N, mostly free from ice. Our assimilation system includes a test that rejects observations situated over sea ice, therefore explaining the negligible impact from 80° to 65°S.

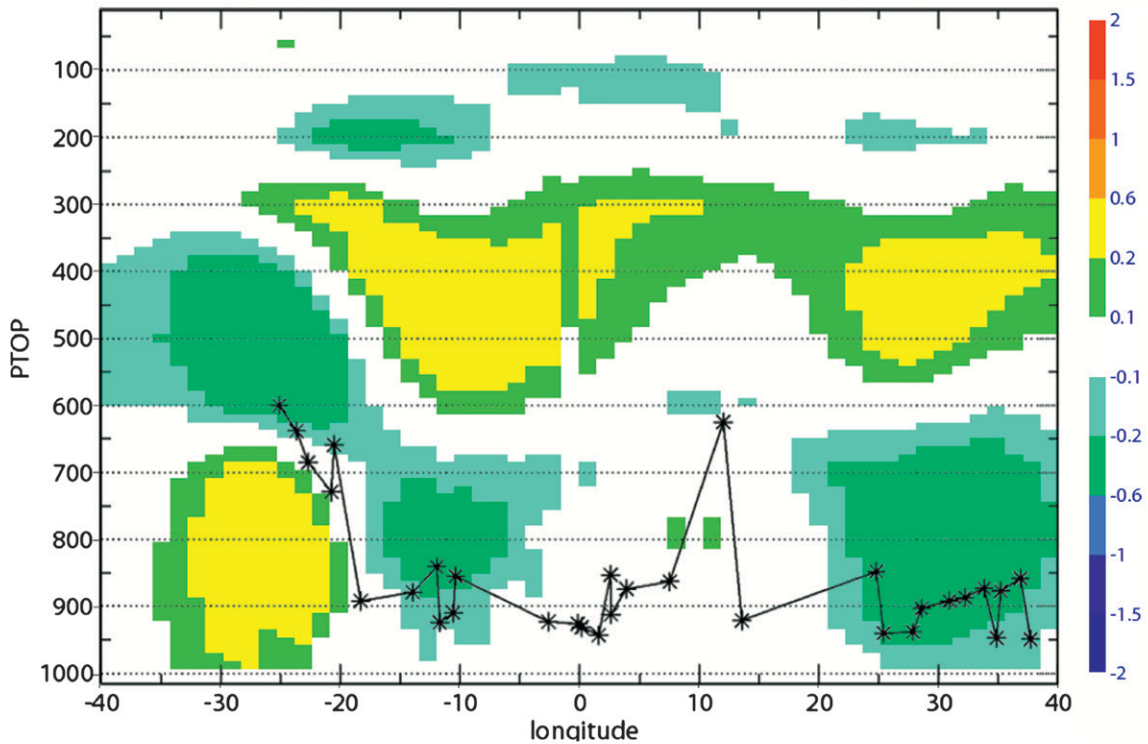
A longitudinal cross section of analysis temperature differences between EXP and REF is shown (Fig. 8b) for the first analysis to characterize the impact of the assimilation of some cloud-affected observations on the analysis with respect to their diagnosed top pressure (from the CO₂ slicing). The cross section at 50°S from 40°W to 40°E is shown because this area displays many active cloud-contaminated observations with different retrieved CTP. From 30° to 20°W, medium clouds are assimilated (600 < CTP < 700 hPa): a warming spreading from the CTP down to the surface is visible. A small cooling is also visible above the CTP up to the upper troposphere (350–400 hPa). From 20°W to 0° and from 20° to 40°E, very low clouds are assimilated (900 < CTP < 950 hPa): a small cooling is visible just above the CTP spreading within the whole lower troposphere (until 650–700 hPa). The upper troposphere is also affected from 600 to 300 hPa: a warming is indeed observed. For very low clouds, these changes can also be accompanied by a slight cooling of the tropopause. Even if these changes highlight the capacity of the cloud-affected radiances to modify the analysis, the lack of verifying data prevents us from assessing which analysis better fits the real state of the atmosphere.

b. Impact on forecasts

The impact of the assimilation of cloud-affected radiances on global forecasts was determined by comparing the objective forecast scores in terms of RMS errors with respect to radiosonde observations. Table 1 shows the RMS forecast error differences for the geopotential



(a) Analysis differences at 500hPa



(b) Cross-section of analysis differences.

FIG. 8. Analysis differences between REF and EXP for temperature at 0000 UTC 1 Sep 2006. (a) The 500-hPa level. Brown circles indicate places where cloud-contaminated pixels are assimilated and the red line at 50°S indicates the location of the cross section shown in (b). The longitudinal cross section is at 50°S and from 40°W to 40°E (shaded colors) and shows the corresponding cloud-top pressure for the assimilated cloud-affected radiances.

TABLE 1. RMS errors of the differences (%) between the geopotential forecast by EXP and REF for a 4-day forecast range with respect to radiosonde observations. Results are averaged from 0000 UTC 1 Sep to 1800 UTC 4 Oct 2006. Boldface indicates a positive impact and regular font indicates a negative impact. Italics indicate values that are statistically significant.

Verifications Domain	Level (hPa)	Forecast range			
		24	48	72	96
20°N (>20°N)	100	0.2	0.5	0.6	0.4
	250	0.31	1.5	1.9	0.9
	500	0.0	0.35	2.3	0.8
	850	-0.2	-0.2	2.2	0.3
20°S (<20°S)	100	0.5	1.1	0.8	-0.2
	250	0.2	1.2	-1.8	-0.5
	500	0.7	1.1	-1.0	1.4
	850	1.3	2.4	-0.1	0.0
Tropics (20°N, 20°S)	100	0.7	0.7	0.4	0.0
	250	0.0	-0.1	0.0	-0.5
	500	0.5	0.4	0.6	-0.1
	850	0.2	0.7	0.8	0.6
Europe	100	1.6	2.0	2.0	0.1
	250	0.2	4.1	4.7	-0.4
	500	0.0	3.5	6.9	-0.9
	850	-0.3	2.6	6.7	-1.2

height. These errors have been computed with respect to radiosonde observations for the validation period ranging from 0000 UTC 1 September 2006 to 1800 UTC 4 October 2006. The impact is rather neutral to slightly positive. The most significant improvement was obtained for the geopotential height according to a statistical Student's *t* test with respect to radiosonde observations with a level of confidence of 95%. Over the Northern Hemisphere, positive impacts are found for a 24–96-h forecast range in the stratosphere and in the mid- to upper troposphere. Improvements at 100 and 250 hPa for a 48-h forecast range are statistically significant. Over the Southern Hemisphere, a positive impact is found for a 24–48-h forecast range in the whole atmosphere. These improvements are significant at the 24–48-h forecast range at 850 and 250 hPa and for the 48–72-h forecast range at 100 hPa. A negative impact has been observed at longer forecast ranges but it is not statistically significant. Over the tropics, positive impacts are found for the 24–72-h forecast range in the stratosphere and in the mid- to low troposphere. These improvements are significant at 850 and 100 hPa for the 24–48-h forecast range. Over Europe, the impact is mainly positive until the 72-h forecast range in the whole atmosphere and negative for the 96-h forecast range. These positive impacts are larger than for the other domains but only significant at 100 hPa at the 48-h forecast range. Scores with respect to ECMWF analyses are rather neutral to slightly positive.

Regarding the other parameters (temperature, humidity, and wind), impacts are roughly neutral to slightly

positive but not significant with respect to radiosonde observations and ECMWF analyses. Similar results were found over another 3-week period (from 0000 UTC 29 May to 1800 UTC 20 June 2008) in a different context: more satellite data were assimilated (ATOVS from *MetOp*, IASI, and GPS radio occultation observations) and the model resolution was higher.

Figures 9a–d represent RMS errors and biases of the 48-h forecast over Europe for the geopotential, temperature, humidity, and wind, respectively. The geopotential is improved in terms of RMS in the whole atmosphere and in terms of bias in the stratosphere. These improvements are significant from 10 to 200 hPa. The temperature is slightly improved in terms of bias and RMS errors from the surface to the tropopause with significant impacts at 200 hPa. The humidity is slightly improved in terms of RMS in the upper troposphere and in the tropopause but not significantly. The wind is improved in terms of RMS errors from the surface to the tropopause and from the upper troposphere to the tropopause in terms of bias. These improvements are significant from 100 to 200 hPa.

The impact of the assimilation of cloud-affected observations on forecasts will now be further discussed by an evaluation of the predictability on a meteorological situation: the so-called Mediterranean hurricane (MEDICANE) case.

6. Case study: The MEDICANE case

a. Synoptic description of the event by ECMWF analyses

On 26 September 2006, a strong mesoscale storm with some resemblance to a polar low hit the southeast part of Italy and caused intense precipitation. This event has been investigated from an observational and a numerical (analysis and forecasts from WRF model) point of view by Moscatello et al. (2008). In this paper, this description has been completed by analyses from the ECMWF model, which will be used as a verification to display the relative performance in terms of predictability of both experiments. The trajectory and the evolution of the mean sea level pressure (MSLP) of the low with respect to each time step are summarized in Fig. 10. ECMWF analyses show that a small-scale cyclone was generated in the southeast of the atlas Tunisian Ridge near the Algerian–Tunisian border at around 0000 UTC 25 September 2006 with a MSLP of about 1007 hPa (Fig. 11a). During the following 18 h, the low moved through an east–northeastward direction without intensifying to reach eastern Malta Island at some 800 km away from its initial position (Fig. 11b) at 1800 UTC 25 September. At 0000 UTC 26 September, the low entered the Ionian Sea near the Ionian coast of Calabria. At this stage, it began

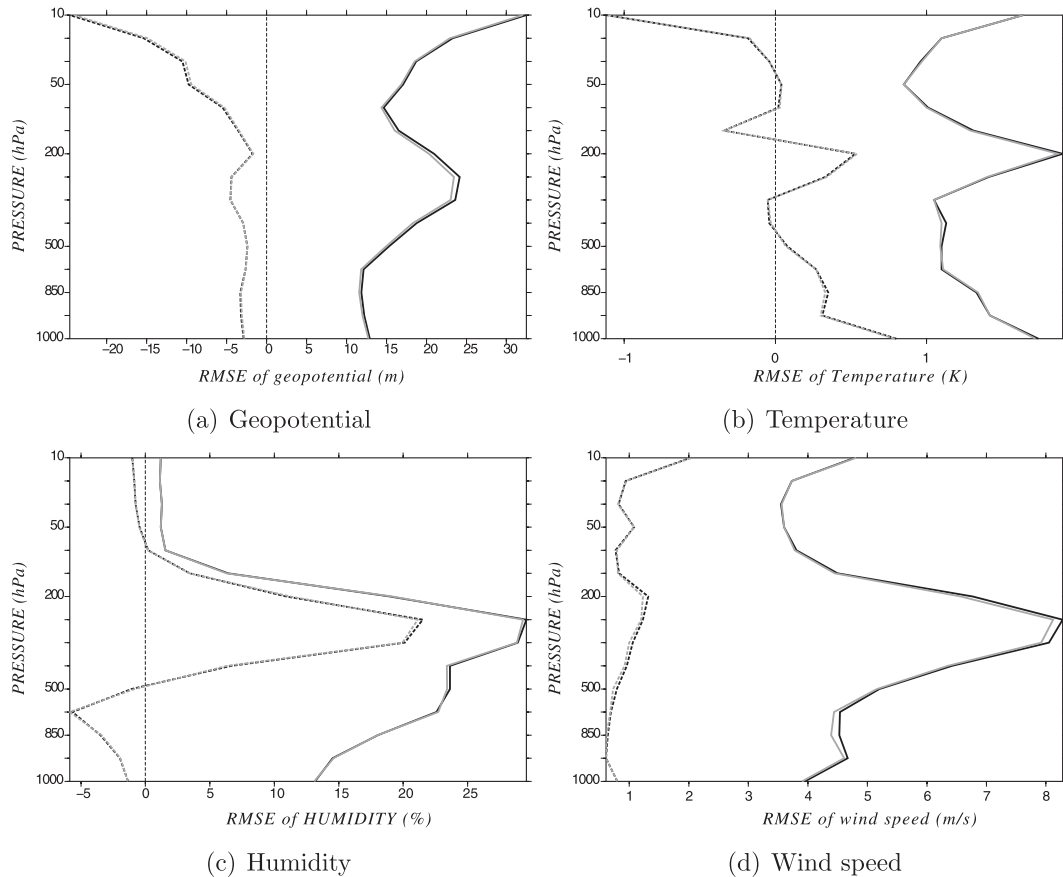


FIG. 9. RMS and mean (bias) of the (a) geopotential, (b) temperature, (c) humidity, and (d) wind differences between 48-h forecasts and radiosonde observations for EXP (gray lines) and REF (black lines) as a function of the pressure. RMS and mean are represented by solid and dashed lines, respectively. Statistics are calculated over the European region and averaged over the period ranging from 0000 UTC 1 Sep to 1800 UTC 4 Oct 2006.

to intensify reaching a MSLP of 1005 hPa. Between 0000 and 0600 UTC, the low moved northeasterly certainly in response to a low pressure system (1001 hPa) visible in the Tyrrhenian Sea (Moscatello et al. 2008) to reach the southern Torento Gulf at 0600 UTC (Fig. 11c). All along this time, the low strongly intensified, reaching a MSLP of about 996 hPa at 0600 UTC. Between 0600 and 1200 UTC, the trajectory of the low curved northward and the depression then crossed the Apulia regions to reach the Adriatic Sea with a MSLP of about 994 hPa, the absolute minimum of the depression at 1200 UTC 26 September. For the next 6 h, the low moved along a northwestward direction and reached the Gargano promontory at 1800 UTC (Fig. 11d) with decreasing intensity (997 hPa). The low then moved inland where it finally died.

b. Predictability of the event

Four sets of numerical simulations have been performed for both experiments in order to compare

the predictability, position, and intensity of the cyclone during its whole development, from 0000 UTC 25 September 2006 to 1800 UTC 26 September 2006.

- 1) The first set, hereinafter called FCST2300, begins at 0000 UTC 23 September 2006 and ends at 1800 UTC 26 September 2006 after a 90-h forecast.
- 2) The second set, FCST2312, begins at 1200 UTC 23 September and ends after a 78-h forecast.
- 3) The third set, FCST2400 begins at 0000 UTC 24 September and ends after a 66-h forecast.
- 4) The fourth set, FCST2412 begins at 1200 UTC 24 September and ends after a 54-h forecast.

Figures 12a–d exhibit the trajectory of the MEDICANE depression forecast by FCST2300, FCST2312, FCST2400, and FCST2412, respectively, ranging from 0000 UTC 25 September 2006 to 1800 UTC 26 September 2006. Forecasts provided by EXP display a better positioning of the low with respect to the ECMWF analyses than REF forecasts for each forecast set and globally for each

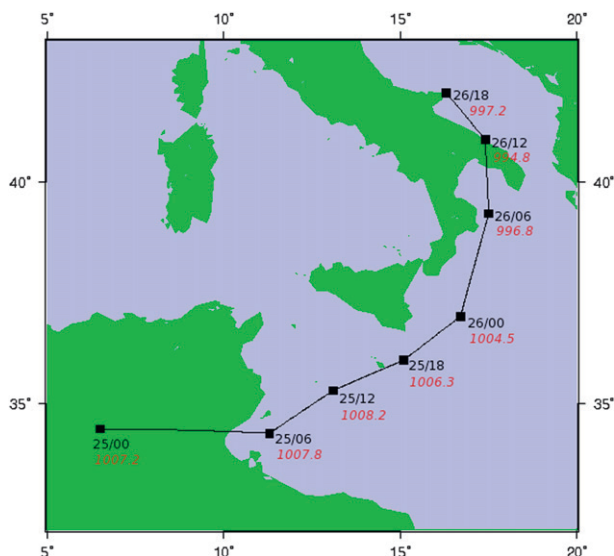


FIG. 10. Trajectory of MEDICANE from ECMWF analysis from 0000 UTC 25 Sep to 1800 UTC 26 Sep 2006. Black numbers indicate the time step and red numbers indicate the corresponding MSLP pressure (hPa).

forecast range. This assessment is true for each time step except for forecasts whose validity date is 1800 UTC 26 September. The position of the low at 1800 UTC 25 September is not forecasted by REF contrary to EXP whichever the considered set. Moreover, the position of the low is neither forecasted by REF at 0000 and 0600 UTC 26 September for the FCST2300 contrary to EXP.

Figures 13a,b highlight the evolution of forecast MSLP minimum by FCST2300 and FCST2312 and FCST2400 and FCST2412, respectively, with respect to the ECMWF analysis. The evolution of the intensity of the low is better forecasted by EXP than REF throughout its whole evolution period for each forecast set. FCST2400 displays the largest averaged difference between EXP and REF (Fig. 13b): differences of MSLP between EXP forecasts and ECMWF analysis are 1.5 hPa on the mean against 3.5 hPa for REF. Furthermore, these differences between EXP and REF tend to grow with the forecast range (at least for FCST2400).

c. Accumulated precipitation

According to Moscatello et al. (2008), the storm caused intense precipitation over the southeastern part of Italy. The first MEDICANE landfall occurs between 0600 and 1200 UTC 26 September 2006 over the Salentine Peninsula. Equitable threat scores (ETS), which are defined as the intersection of the forecast and observations divided by the union of the forecast and observations at a given threshold, have thus been calculated (Fig. 14). These scores highlight forecast performance of both ex-

periments in terms of cumulated precipitation (within a 6-h window). The closer the score is to 1, the better the forecast. These scores are calculated with respect to cumulated precipitation observations (SYNOP situated between 28° and 55°N and between 0° and 30°E) available from 0600 to 1200 UTC 26 September 2006 for four different threshold (0.1, 1, 5, and 10 mm) and according to seven different forecast ranges (6, 12, 36, 48, 60, 72, and 84 h).

For very low precipitation (threshold = 0.1 mm), performances of both experiments are quite bad at each forecast range (not shown) but they are slightly improved in EXP. The same assessment can be made regarding a threshold of precipitations of 1 mm (not shown). However, for longtime forecast ranges (from 72 to 84 h), performances of REF are slightly better than EXP for this threshold. As can be seen in Figs. 14a,b, regarding thresholds of 5 mm (steady precipitation) and 10 mm (strong precipitation), respectively, EXP globally exhibits better scores with respect to observations than does REF. For steady precipitation (threshold = 5 mm), performances of both experiments are better than for lower precipitations (Fig. 14a) with better performances of EXP at each forecast range except for the 84-h forecast range. Regarding stronger precipitation (threshold = 10 mm), both performances are reasonable (Fig. 14b) but EXP also exhibits better performances at each forecast range. Cumulated precipitation forecasts are thus improved whatever the rainfall rate but especially for steady and strong precipitation.

7. Conclusions and future developments

The ARPEGE 4D-Var assimilation system has been modified to directly assimilate some AIRS cloud-affected radiances in addition to clear ones. Once a cloud-affected pixel is detected by the CO₂-slicing scheme, cloud parameters (CTP and N_e) are retrieved and directly provided to RTTOV, which will then simulate the cloud-affected spectrum. Furthermore, the ECMWF scheme identifies each clear and cloudy channel of the pixel. Finally, channels affected by clouds whose CTP ranges between 600 and 950 hPa are assimilated in addition to clear ones. All other cloud-contaminated channels are rejected from the assimilation scheme.

ECMWF and CO₂-slicing schemes have been evaluated using independent MODIS data. It has been found that both schemes were performing well in terms of cloud detection. Both cloud-detection performances fluctuate with respect to the diagnosed height of the considered cloud: medium clouds (400 < CTP < 800 hPa) are best detected whereas the detection of low and very low clouds is not very efficient. However, it has also been

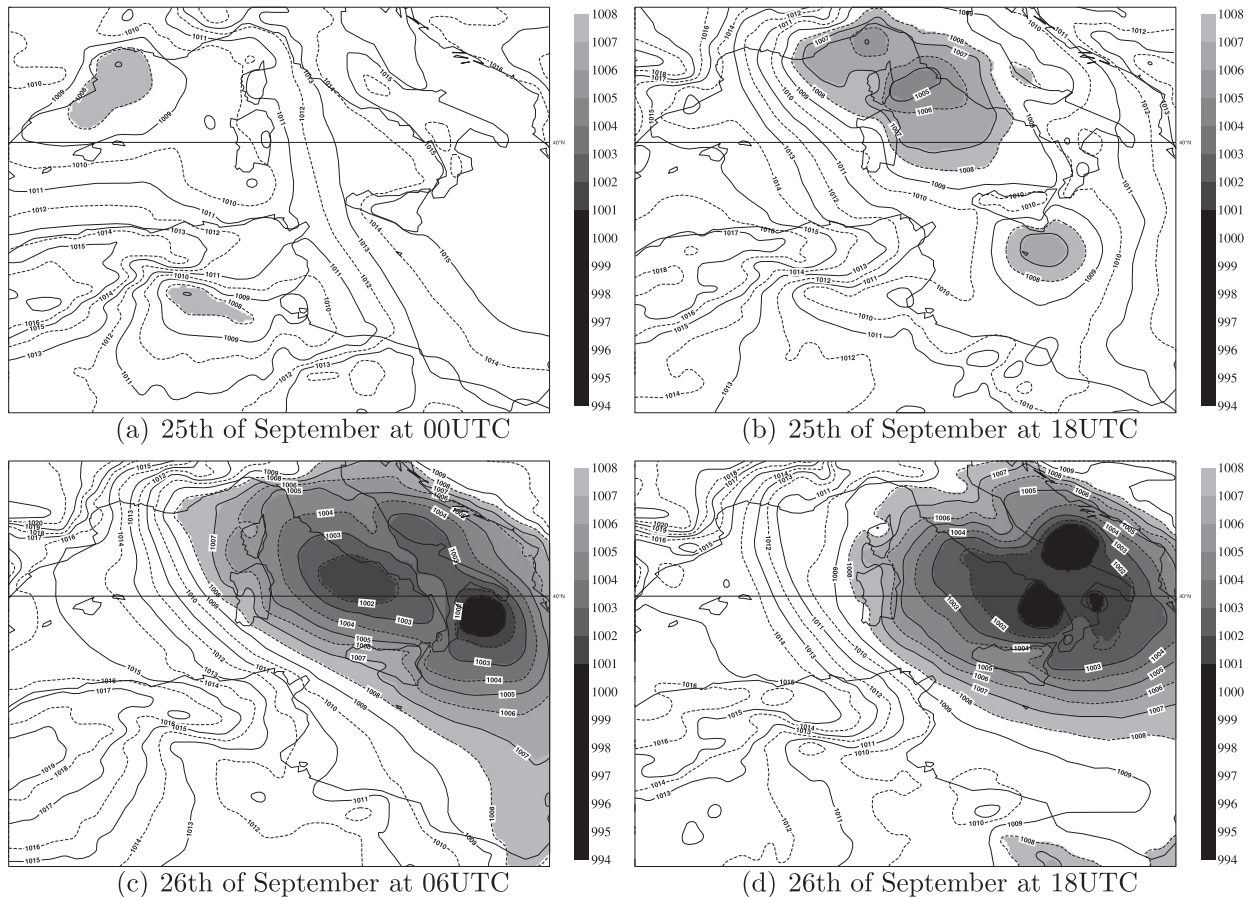


FIG. 11. Analyses of MEDICANE by the operational ECMWF model for 0000 UTC 25 Sep to 1800 UTC 26 Sep 2006. Contours are MSLP (interval of 1 hPa) and shading indicates values <1006 hPa.

demonstrated that difficulties of cloud-detection schemes to detect some low-level clouds have a negligible impact on the simulation of observations contrary to the other levels of clouds. The retrieved cloud-top pressure from CO_2 slicing exhibits a good correlation with the cloud-top pressure inferred from MODIS. The retrieved effective cloud fraction exhibits lower correlations with the effective cloud fraction inferred from MODIS.

Assimilation experiments have been run with the new assimilation scheme: on average, 3.5% of additional pixels are assimilated over the globe with quite a uniform geographic repartition but additional assimilated channels are much more numerous for mid- to high latitudes (10% of additional assimilated channels on average). These extra assimilated data first affect the simulation of model equivalents, which are more consistent with observations as shown by the significant reduction of innovations, especially for longwave surface peaking channels and shortwave channels. Second, the assimilation of cloud-affected observations in addition to clear ones permits the analysis and the back-

ground to better fit some conventional observations such as wind profilers and some satellite data sensitive to the atmospheric humidity, such as SSM/I and AMSU-B in terms of bias and RMS errors. Finally, analysis model fields are affected, especially where the extra data volume is important (e.g., mid- to high latitudes). Changes within the atmosphere column differ in accordance with the diagnosed height of the assimilated cloud.

Global forecasts using cloud-contaminated observations have been performed for two validation periods: impacts are rather neutral to slightly positive for each parameter over all domains and for both validation periods. However, they are on the whole not significant except for the geopotential where significant improvements have been highlighted for the 24–48-h forecast range in the stratosphere and in the high troposphere over each domain and in the low troposphere over the tropics and the Southern Hemisphere.

The new assimilation scheme has also been tested on a practical study case: MEDICANE, a strong mesoscale storm, which hit the southeast part of Italy on the

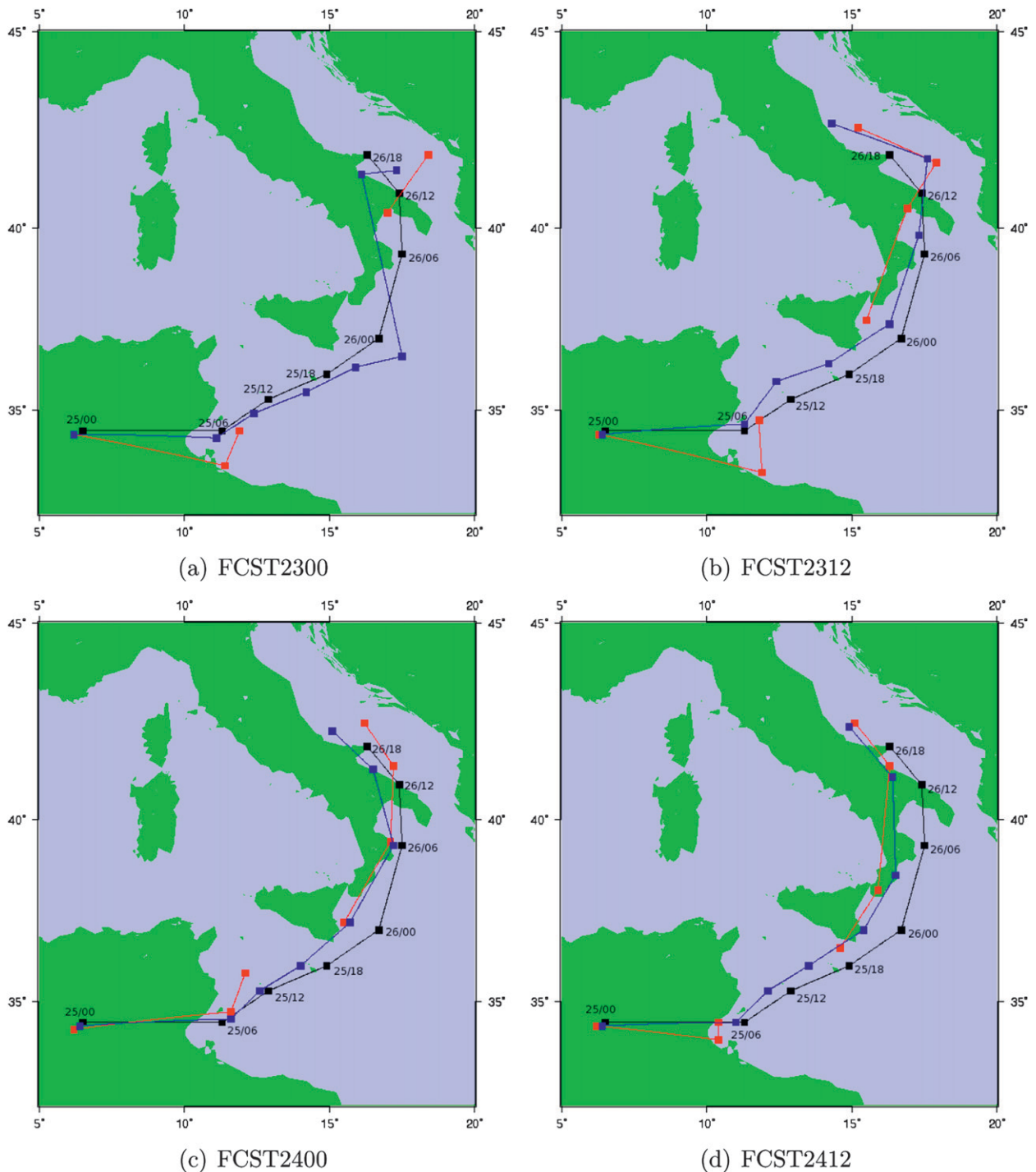


FIG. 12. Trajectory of MEDICANE from (a) FCST2300, (b) FCST2312, (c) FCST2400, and (d) FCST2412. The lines represent the trajectories forecasted by REF (red) and EXP (blue), and given by the ECMWF analysis (black). Black numbers indicate the corresponding time step of MEDICANE.

26 September 2006. Forecasts run from the analysis using cloud-affected radiances are improved with respect to those assimilating only clear ones: the trajectory, intensity, and whole development of the low are better

predicted for all the forecast range. Cumulated precipitation forecasts are also improved whatever the rate of rainfall but especially for steady and strong precipitation.

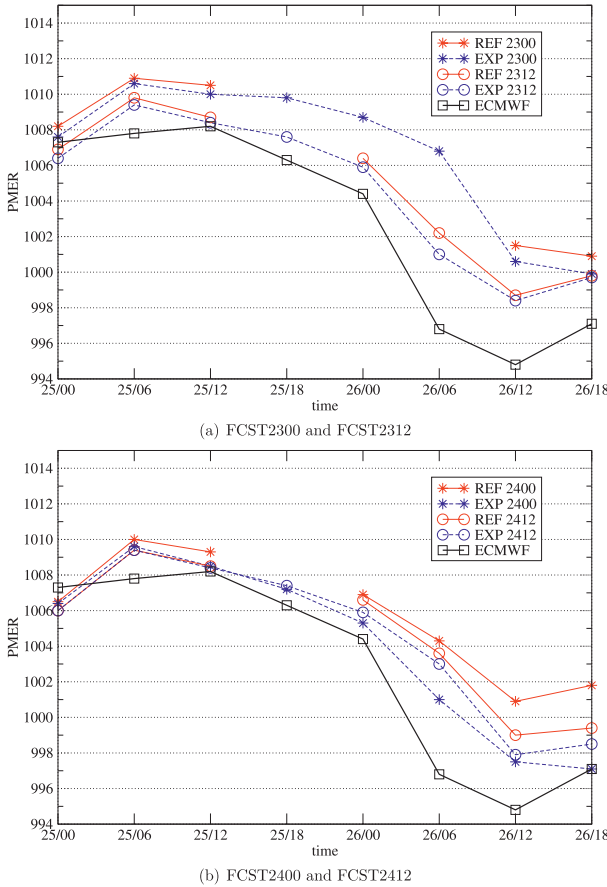


FIG. 13. Evolution of the minimum of MSLP from 0000 UTC 25 Sep to 1800 UTC 26 Sep 2006. Black line with squares represents the trajectory from ECMWF, dashed blue lines represent the evolution from EXP, and solid red lines represent the evolution from REF. (a) Stars (circles) represent FCST2300 (FCST2312). (b) Stars (circles) represent FCST2400 (FCST2412).

Although results presented in this paper are encouraging, several issues are still to be addressed. First, the bias correction used for clear radiances is applied to cloud-affected radiances and the corrections required should differ from cloud-affected to clear observations. Second, cloud parameters are directly provided to RTTOV in the current assimilation scheme. A prior adjustment by a 1D-Var scheme could admittedly slightly improve the assimilation scheme (Dahoui 2006; Pavelin et al. 2008) but this method, besides being expensive in calculation time, may create discrepancies between cloud parameters and other control variables. The adjustment of cloud parameters inside the iterative process of the 4D-Var could lead to more consistent cloud parameters with other variables. Finally, the rejection of cloud-affected channels whose CTP is situated above 600 hPa leads to a rather low yield in terms of additional active data. Experiments assimilating clouds up to 400 hPa (with

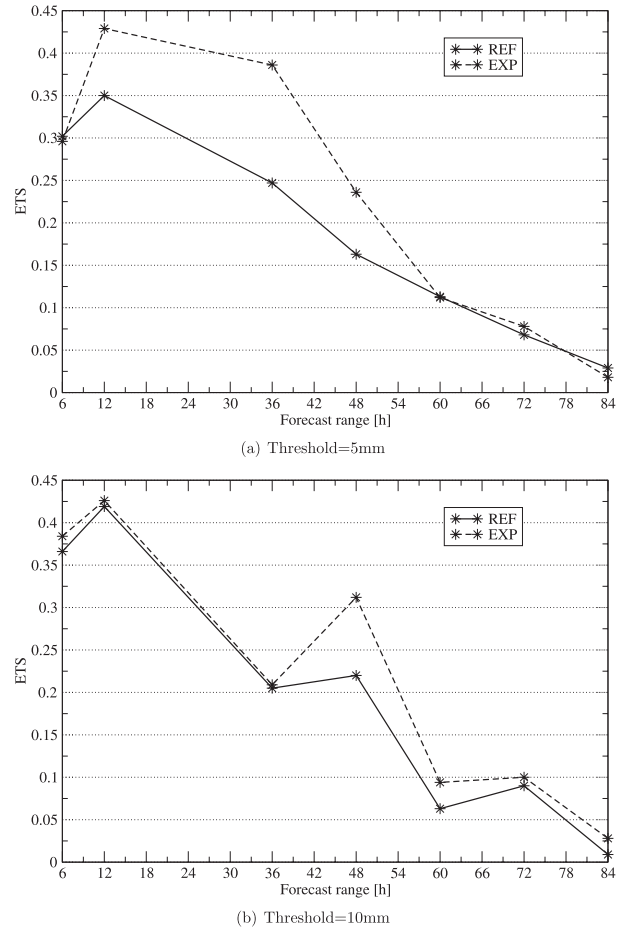


FIG. 14. ETS for EXP and REF with respect to the forecast range for thresholds of 5 and 10 mm between 0600 and 1200 UTC 26 Sep 2006. Solid line represents the REF and the dashed line represents the EXP.

a rejection of channels whose weighting-function peak is below the CTP) have been run with a rather neutral (to negative) impact on forecasts. The assimilation of these kinds of clouds thus requires additional developments.

This new assimilation method is obviously valid for other advanced sounders and regarding the short-term development of the approach described in this paper, the next step will be to extend this cloud-affected radiance assimilation scheme to IASI data. Its higher spectral resolution could lead to promising results.

On February 2009, the new assimilation scheme described here was implemented in the operational data assimilation configuration at Météo-France.

Acknowledgments. The authors express their thanks to the ICARE Centre for providing MODIS cloud data products used to evaluate the cloud-detection schemes. In addition, Jean Maziejewski and Fatima Karbou are warmly thanked for their helpful comments on

a previous version of this manuscript. The authors are also grateful to Alexis Doerenbecher and Frank Guillaume for providing many improvements on the quality of figures presented in this work. Finally, we thank the two anonymous reviewers for their constructive comments.

REFERENCES

- Auligné, T., T. McNally, and D. Dee, 2007: Adaptive bias correction for satellite data in a numerical weather prediction system. *Quart. J. Roy. Meteor. Soc.*, **133**, 631–642.
- Aumann, H., and Coauthors, 2003: AIRS/AMSU/HSB on the Aqua mission: Design, science objectives, data products and processing systems. *IEEE Trans. Geosci. Remote Sens.*, **41** (2), 253–264.
- Cayla, F., 2001: L'interféromètre iasi; un nouveau sondeur satellitaire haute résolution (The IASI interferometer: A new high-resolution satellite sounder). *La Météorologie*, **32**, 23–39.
- Chahine, M., 1974: Remote sounding of cloudy atmospheres. I. The single cloud layer. *J. Atmos. Sci.*, **31**, 233–243.
- Chevallier, F., P. Lopez, A. M. Tompkins, M. Janiskova, and E. Moreau, 2004: The capability of 4d-Var systems to assimilate cloud-affected satellite infrared radiances. *Quart. J. Roy. Meteor. Soc.*, **130**, 917–932.
- Courtier, P., C. Freydl, F. Rabier, and M. Rochas, 1991: The ARPEGE Project at Météo-France. *Proc. ECMWF Seminar on Numerical Methods in Atmospheric Models*, Vol. 7, Reading, United Kingdom, ECMWF, 193–231.
- , J.-N. Thepaut, and A. Hollingsworth, 1994: A strategy for operational implementation of 4D-Var using an incremental approach. *Quart. J. Roy. Meteor. Soc.*, **120**, 1367–1387.
- Dahoui, M. L., 2006: Vers une assimilation variationnelle des radiances satellitaires nuageuses (Toward a variational assimilation of cloudy satellite radiances). Thèse de doctorat, Université Toulouse 3-Paul Sabatier, France, 160 pp.
- , L. Lavanant, F. Rabier, and T. Auligné, 2005: Use of MODIS imager to help dealing with AIRS cloudy radiances. *Quart. J. Roy. Meteor. Soc.*, **131**, 2559–2579.
- Dee, D., 2004: Variational bias correction of radiance data in the ECMWF system. *Proc. ECMWF Workshop on Assimilation of High Spectral Resolution Sounders in NWP*, Reading, United Kingdom, ECMWF, 97–112.
- English, S., J. Eyre, and J. Smith, 1999: A cloud-detection scheme for use with satellite sounding radiances in the context of data assimilation for numerical weather predictions. *Quart. J. Roy. Meteor. Soc.*, **125**, 2359–2378.
- Eyre, J. R., and P. Watts, 1987: A sequential estimation approach to cloud-clearing for satellite temperature sounding. *Quart. J. Roy. Meteor. Soc.*, **113**, 1349–1376.
- , and W. P. Menzel, 1989: Retrieval of cloud parameters from satellite sounder data: A simulation study. *J. Appl. Meteor.*, **28**, 267–275.
- Fourrié, N., and F. Rabier, 2004: Cloud characteristics and channel selection for IASI radiances in meteorologically sensitive areas. *Quart. J. Roy. Meteor. Soc.*, **130**, 1839–1856.
- Li, J., C. Liu, H. L. Huang, T. J. Schmit, X. Wu, and W. P. Menzel, 2005: Optimal cloud-clearing for AIRS radiances using MODIS. *IEEE Trans. Geosci. Remote Sens.*, **43**, 1266–1278.
- McNally, A., 2002: A note on the occurrence of cloud in meteorologically sensitive areas and the implications for advanced infrared sounders. *Quart. J. Roy. Meteor. Soc.*, **128**, 2551–2556.
- , and P. Watts, 2003: A cloud detection algorithm for high spectral resolution infrared sounders. *Quart. J. Roy. Meteor. Soc.*, **129**, 3411–3423.
- Menzel, W., T. Smith, and T. R. Stewart, 1983: Improved cloud motion wind vector and altitude assignment using VAS. *J. Climate Appl. Meteor.*, **22**, 377–384.
- Moscattello, A., M. Marcello Miglietta, and R. Rotunno, 2008: Numerical analysis of a Mediterranean “hurricane” over southeastern Italy. *Mon. Wea. Rev.*, **136**, 4373–4397.
- Pavelin, E., S. English, and J. Eyre, 2008: The assimilation of cloud-affected infrared satellite radiances for numerical weather prediction. *Quart. J. Roy. Meteor. Soc.*, **134**, 737–749.
- Rabier, F., H. Järvinen, E. Klinker, J.-F. Mahfouf, and A. Simmons, 2000: The ECMWF operational implementation of four-dimensional variational assimilation. I: Experimental results with simplified physics. *Quart. J. Roy. Meteor. Soc.*, **126**, 1143–1170.
- Saunders, R. W., P. Brunel, G. Chevallier, F. Deblonde, M. English, S. Matricardi, and P. J. Rayer, 2002: RTTOV-7 science and validation report. NWP Forecasting Research Tech. Rep. 387, 51 pp.